

# Voltage Induced Hidden Symmetry and Photon Entanglement Generation in a Single, Site-Selected Quantum Dot

M. E. Reimer,<sup>1,2</sup> M. Korkusiński,<sup>1</sup> J. Lefebvre,<sup>1</sup> J. Lapointe,<sup>1</sup> P. J. Poole,<sup>1</sup> G. C. Aers,<sup>1</sup>  
D. Dalacu,<sup>1</sup> W. R. McKinnon,<sup>1</sup> S. Frédérick,<sup>1,2</sup> P. Hawrylak,<sup>1,2</sup> and R. L. Williams<sup>1,2</sup>

<sup>1</sup>*Institute for Microstructural Sciences, National Research Council of Canada, Ottawa, Ontario, Canada K1A 0R6*

<sup>2</sup>*Department of Physics, University of Ottawa, Ottawa, Ontario, Canada K1N 6N5*

(Dated: October 24, 2018)

Present proposals for the realisation of entangled photon pair sources using the radiative decay of the biexciton in semiconductor quantum dots are limited by the need to enforce degeneracy of the two intermediate, single exciton states. We show how this requirement is lifted if the biexciton binding energy can be tuned to zero and we demonstrate this unbinding of the biexciton in a single, pre-positioned InAs quantum dot subject to a lateral electric field. Full Configuration-Interaction calculations are presented that reveal how the biexciton is unbound through manipulation of the electron-hole Coulomb interaction and the consequent introduction of Hidden Symmetry.

PACS numbers: 78.67.Hc, 78.55.-m, 85.35.Be, 03.65.Ud

Site-selected InAs/InP quantum dots emitting in the wavelength range between 1300 nm and 1550 nm offer a fully scalable route to sources of single photons and entangled photon pairs for fibre-based quantum cryptography [1, 2, 3, 4, 5], quantum teleportation [6] and quantum repeater technologies [7]. In such strongly confined systems, the Coulomb interactions between optically generated electrons and holes, as well as the dot size and compositional structure, play a major role in determining transition energies and oscillator strengths. Presently, in order to produce polarisation entangled photon pairs, the biexciton radiative decay cascade in single semiconductor quantum dots (QDs) [4, 8, 9] is utilized. Entanglement in these schemes is destroyed however if the degeneracy of the two possible spin configurations of the intermediate neutral exciton ground state is lifted, as is frequently the case in the presence of the electron-hole exchange interaction in anisotropic quantum dots [10]. As such, there have been extensive efforts to remove the anisotropic exchange splitting (AES) through the application of external magnetic [8] and electric [11, 12] fields or through spectral filtering [9] and quantum dot size and composition engineering [13].

In this Letter, we propose an alternative scheme for entangled photon pair generation from quantum dots (QDs) that is robust to the presence of anisotropic exchange splitting. By precisely balancing the competing Coulomb attractions and repulsions for excitons ( $X$ ) and biexcitons ( $XX$ ) within a single InAs/InP QD using an applied lateral electric field, we enforce Hidden Symmetry [14, 15, 16] within the dot. Under such circumstances, the binding energy of the biexciton vanishes and it is possible to identify two indistinguishable recombination pathways for the biexciton, even in the presence of non-degenerate intermediate exciton states. The observed behavior allows us to identify a voltage controlled route to entangled photon pair generation even from imperfect QDs, without resort to large external magnetic fields, or

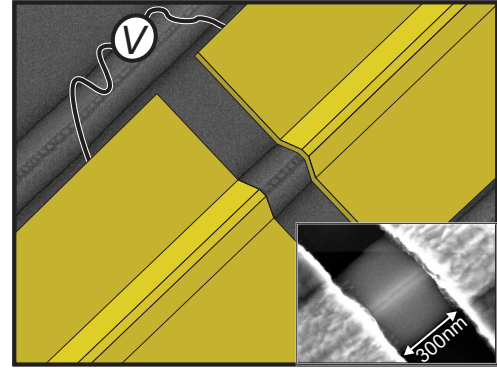


FIG. 1: (Color Online) Schematic view of the device showing two metallic gates on top of an SEM micrograph of an uncapped, "stripe geometry" InP ridge. A linear array of InAs QDs is seen at the apex of the ridge, in the space separating the gates. In real devices, the QDs are capped with InP prior to gate deposition, as shown in the inset SEM micrograph, and the dot density is chosen to be lower than that shown for the uncapped sample, so that individual dots can be isolated.

materials engineering of individual dots.

Fig. 1 shows a schematic view of the sample construction used here to apply a lateral electric field to single InAs/InP QDs. Dots are nucleated at the apex of a "stripe geometry" InP nanotemplate and subsequently capped with InP. Such templates, produced *in situ* during crystal growth, allow one to control the surface migration of deposited InAs, so that the nucleation site of the dots can be selected *a priori* [17]. Pairs of metallic, Schottky gates, deposited across the InP nanotemplate, with narrow ( $\sim 300$  nm) gaps, allow in-plane electric fields to be applied along the stripe (x-) direction and serve to isolate the luminescence from individual QDs if the dot density is sufficiently low.

Photoluminescence experiments were performed under applied electric field, with an excitation intensity chosen

to excite only the ground state transition from the QD at zero applied electric field. Low excitation intensity was required to ensure minimal screening of the applied electric field.

To demonstrate the manipulation of the biexciton binding energy and the engineering of Hidden Symmetry, we select an InAs/InP QD that exhibits a negative  $XX$  binding energy at zero applied bias. Photoluminescence data from such a dot as a function of the applied lateral electric field is shown in Fig. 2, with the appearance of the  $XX$  at lower energy than the  $X$  shown in the inset, at zero electric field and higher excitation power. At zero applied bias, transitions from the two neutral exciton ground states, split by e-h exchange, are observed at approximately 922.4 meV (1344 nm). For biases from 0 V to approximately 1.9 V, the mean  $X$  energy shows a surprisingly small Stark shift, that will be discussed subsequently, whilst the AES diminishes from 108  $\mu\text{eV}$  to 56  $\mu\text{eV}$ . Beyond 1.9 V, the AES is below the instrumental resolution (50  $\mu\text{eV}$ ) and the oscillator strength of the  $X$  decays monotonically. Both the zero field value of the AES and its reduction with the applied lateral field are consistent with the behavior observed previously for InAs/GaAs QDs by Kowalik and co-workers [15]. At approximately 1.9 V, the slowly red shifting  $X$  transition is crossed by a peak that blue shifts with further increases in bias and a pair of peaks appear approximately 5 meV above the  $X$ . This behavior is shown more clearly in Fig. 3a, where the peak positions have been extracted from Fig. 2. The general behavior discussed here is typical of single InAs/InP QDs nucleated on "strip geometry" templates and has been observed on eight separate QDs nucleated on templates with a variety of widths. The observed behavior is generally insensitive to the direction of the applied electric field, although the Schottky contacts are sometimes "leaky" in one direction, preventing the application of an electric field in this direction.

To understand the effects of the lateral electric field, we model the QD using an isotropic, two-dimensional, parabolic confining potential in the plane and calculate the expected emission energies and intensities within the Full Configuration Interaction (CI) approach. This involves constructing all possible configurations of  $N_e$  electrons and  $N_h$  holes on the single-particle states in the three lowest lying shells ( $s$ ,  $p$ ,  $d$ ), forming the Hamiltonian matrix in the basis of these configurations, and diagonalizing it numerically. Using the resulting excitonic eigenenergies and eigenvalues, we calculate the emission spectrum using Fermi's Golden Rule,  $I(\omega) = \sum_f |\langle f, N_e - 1, N_h - 1 | P^- | i, N_e, N_h \rangle|^2 \delta(E_i - E_f - \hbar\omega)$ , where  $P^-$  is the interband polarization operator removing one electron-hole pair from the system,  $P^- = \sum_{ij} \alpha_{ij} c_i h_j$ , and  $\alpha_{ij} = {}_e \langle i | j \rangle_h$  is the overlap integral, controlling the optical selection rules for the emission. Here,  $c_i$ ,  $h_j$  represent the the electron and hole annihilation operators, respectively. The Hamiltonian uti-

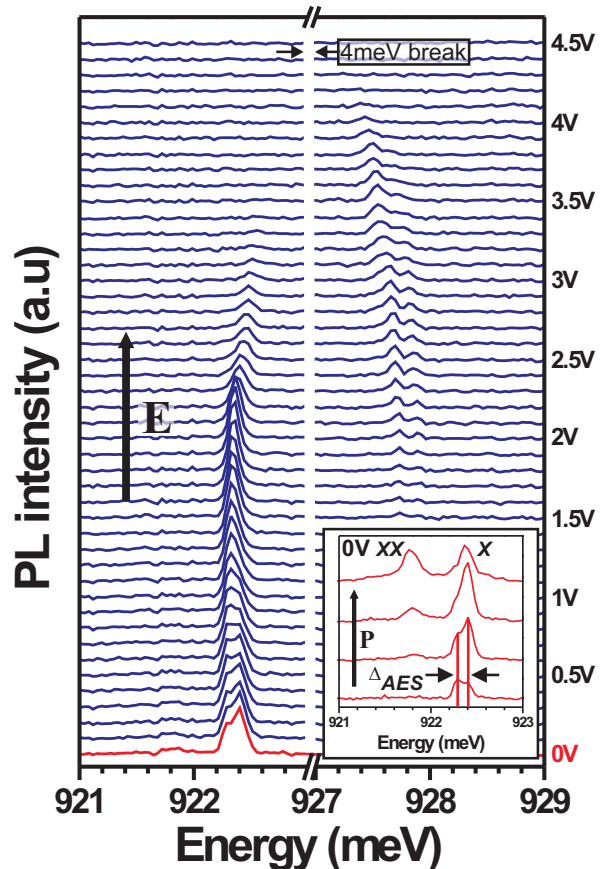


FIG. 2: (Color Online) Electric field dependent PL spectra at  $T = 4.2$  K. There is a 4 meV break from 923 meV to 927 meV. (Inset) Power dependent PL at 0 V. The biexciton ( $XX$ ), identified by its quadratic power dependence, is observed at lower energy than the exciton ( $X$ ) and has a binding energy of 510  $\mu\text{eV}$ .

lized for the interacting electrons and holes confined in the QD can be found in ref [15]. In addition we add a term to the Hamiltonian that describes the electron-hole exchange effects. In this work we use the effective exchange Hamiltonian as described in Ref. [10]. The results of these calculations are shown in Fig. 3b, for the ground and excited (forbidden) state of the neutral exciton and for the ground state of the biexciton. At zero applied electric field, the neutral exciton transitions correspond to the recombination of a single electron and hole in the  $s$ -shell of a parabolic QD. For an electric field  $E$  applied along the  $x$  axis, the confining potential in the  $x$  direction,  $V(x) = \frac{1}{2}m_e^*w_e^2x^2 - eEx$ , remains parabolic,  $V(x) = \frac{1}{2}m_e^*w_e^2(x - \Delta x_e)^2 - \Delta \varepsilon_e$ , with a spatial shift  $\Delta x_e = +eE/m_e^*w_e^2$  for the electron and  $\Delta x_h = +eE/m_h^*w_h^2$  for the hole. Here  $e$  and  $m_e$  are the electron charge and effective mass respectively and  $\hbar w_e$  is the characteristic energy of the confinement. The equivalent hole parameters are labeled by the subscript  $h$ . The relative shift of the origins of electron and hole

confinements results in a change of overlaps between electron and hole states, influencing the oscillator strength of the transitions. In the calculations presented here we assume the following system parameters:  $\hbar w_e = 12$  meV,  $m_e^* = 0.055m_0$ ,  $\hbar w_h = 6$  meV, and  $m_h^* = 0.11m_0$  with  $m_0$  being the mass of a free electron. Under applied lateral field, the induced e-h charge separation produces a reduction in the  $X$  oscillator strength and allows transitions between s-shell electrons and p-shell holes ( $s - p_x$ ) that were symmetry forbidden at zero electric field. The predicted behavior allows us to identify the two peaks appearing in experiment under bias, approximately 5 meV above the  $X$ , as  $s - p_x$  and  $s - p_y$  transitions from a slightly asymmetric QD in which the electric field does not coincide exactly with either of the QD axes. For the  $X$  transitions, the CI calculations predict a monotonic decrease of the AES with applied electric field, as observed experimentally, and a Stark shift that is finite, but much smaller than that expected for a non-interacting electron-hole pair. In addition to the red shifting  $X$ ,  $s - p_x$  and  $s - p_y$  transitions, the CI calculations predict a blue shift in the  $XX$  transition with increasing electric field and an eventual crossing of the  $X$  and  $XX$  transition energies. At this crossing point the binding energy of the  $XX$  vanishes ( $B.E._{XX} = 0$ ) and the QD displays Hidden Symmetry. In experiment, the crossing of the  $X$  and  $XX$  is observed at approximately 1.9 V and the  $XX$  blue shift is observed above this. The appearance of the  $XX$  at the low excitation powers used here to avoid screening effects, is somewhat surprising, but might be expected due to the increased radiative lifetime of the  $X$  as charge separates under the applied field [18].

For a source of entangled photon pairs, the benefit of voltage induced Hidden Symmetry is shown in Fig 4. Within existing proposals, the two channels for biexciton decay ( $A$  and  $B$ ) are made indistinguishable by setting  $\Delta_{AES} = 0$ , so that transitions  $A_1$  and  $B_1$  in Fig. 4a become degenerate, as well as the transitions  $A_2$  and  $B_2$ . Removal of the AES for arrays of individual QDs is technologically difficult however since the application of large magnetic fields [8] or compositional modifications [13] cannot be done locally on a dot to dot basis. However, considering Fig. 4b, it is clear that in the presence of Hidden symmetry, where  $\Delta E_{XX} = \Delta E_X$ , we may identify two pairs of degenerate transitions even in the presence of a non-zero AES:  $A_1$  and  $B_2$ , as well as  $A_2$  and  $B_1$ . This behavior restores the indistinguishability of the biexciton decay channels and suggests that arrays of individually addressable, voltage controlled QDs would be able to provide multiple sources of entangled photons, in which the two-photon wave function is entangled in the horizontal ( $H$ ) and vertical ( $V$ ) polarisation degrees of freedom,  $\psi = \frac{1}{\sqrt{2}}(|HH\rangle + |VV\rangle)$ . Within the proposed scheme it would be possible, in principle, to distinguish the decay channel if temporal information were available. However, this objection is unfounded since a combination

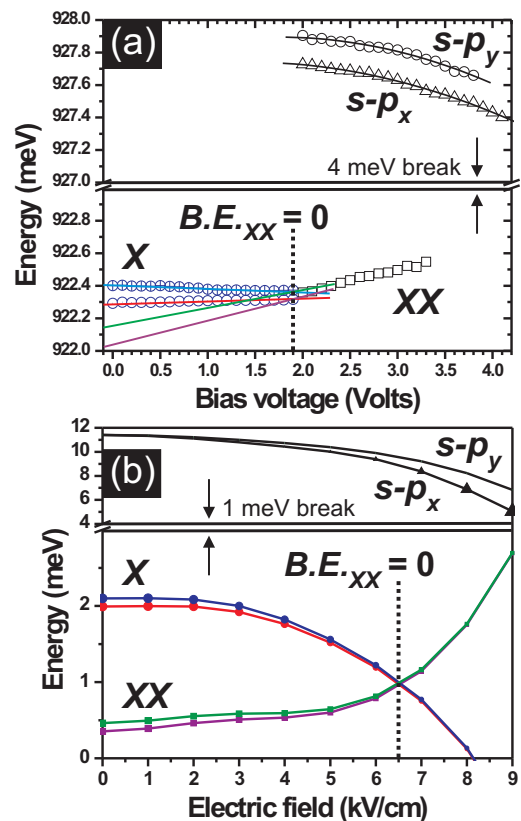


FIG. 3: (Color Online) Tuning of the biexciton binding energy to zero ( $B.E._{XX} = 0$ ). (a) Peak energies extracted from Fig. 2 as a function of the electric field (bias voltage). The AES splitting of the exciton,  $X$ , (open blue circles) diminishes with increasing bias until the biexciton,  $XX$ , (open black squares) appears at approximately 1.9 V. Forbidden transitions,  $s - p_x$  (open black triangles) and  $s - p_y$  (open black circles) are shown with a quadratic fit (solid black line). Transitions from Fig. 4 are shown schematically with the experimental data. (b) Calculated PL transitions as a function of lateral electric field obtained from Fermi's golden rule. Symbols size ( $\times 10$  for  $s - p_x$ ,  $s - p_y$ ) is used to indicate the size of the e-h overlap. Exciton,  $X$ , and biexciton,  $XX$ , transitions ( $B_1$ ,  $A_1$ ,  $A_2$ ,  $B_2$ ) are colour coded in the same manner used for Fig. 4.

of linear optical elements following the QD, such as polarizing beam splitters, energy filters, and optical delay lines can be used to completely remove any timing information and restore temporal overlap. This removal of the timing information is facilitated by the separation into horizontal and vertical polarizations for both photons on each arm of the  $XX$  decay.

For such a device to operate, the engineered crossing of the  $X$  and  $XX$  lines is critical and can be easily understood. In the absence of e-h exchange, the two optically active exciton states have the same energy,  $E_X = \varepsilon_{00}^e + \varepsilon_{00}^h - V_{eh}^0 - \Delta E_X^{CORR}$ , corresponding to the sum of two single-particle energies,  $\varepsilon_{00}^e + \varepsilon_{00}^h$ , an e-h attraction,  $-V_{eh}^0$ , and the correlation energy,  $\Delta E_X^{CORR}$ . The e-h exchange mixes the two exciton configurations

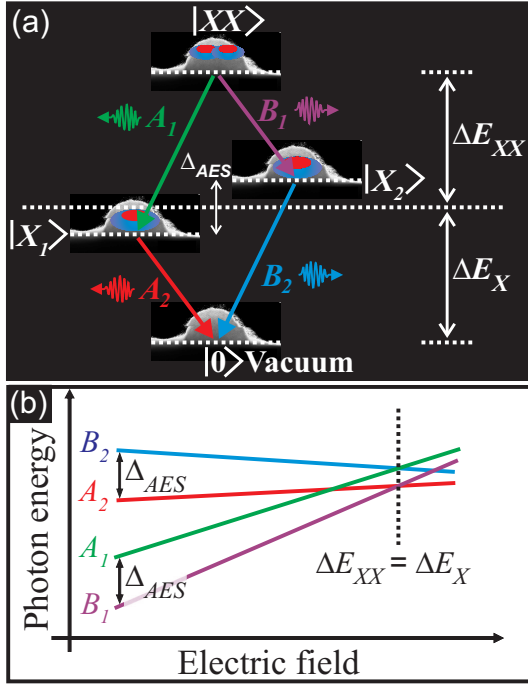


FIG. 4: (Color Online) Polarization entangled photon source exhibiting exchange splitting. (a) Schematic diagram of the biexciton-radiative cascade for a polarization entangled photon source exhibiting an anisotropic exchange splitting (AES) when the binding energy of the biexciton is tuned to zero ( $\Delta E_{xx} = \Delta E_x$ ). Two possible decay paths exist from the biexciton  $|XX\rangle$  to vacuum  $|0\rangle$  through the intermediate, non-degenerate excitonic states  $|X_1\rangle$  and  $|X_2\rangle$ . The solid lines with arrows indicate transitions with energy  $A_1$  (green),  $A_2$  (red),  $B_1$  (purple) and  $B_2$  (blue). The two possible decay paths of the  $XX - X$  cascade are represented by  $A$  and  $B$ , whilst the subscript 1 (2) denotes the first (second) photon emitted in the cascade. (b) Schematic view of transitions in (a) as a function of lateral electric field with the same colour scheme for transitions. For the case when  $\Delta E_{xx} = \Delta E_x$ , the biexciton binding energy vanishes and a polarization entangled photon pair is possible, even in the presence of exchange splitting.

and splits their energies; producing two excitonic states with energies  $E_{X1, X2} = \epsilon_{00}^e + \epsilon_{00}^h - V_{eh}^0 - \Delta E_X^{CORR} \mp \frac{\Delta AES}{2}$ . These are the intermediate states in the biexciton cascade, shown schematically in Fig. 4a. Since the final state in the excitonic recombination is the vacuum, the above energies also define the PL peak positions corresponding to the transitions  $A_2$  and  $B_2$ . As the electrostatic field  $E$  is increased, both single-particle terms decrease due to the Stark effect. However, detailed calculations [19] show that  $V_{eh}^0$  and the correlation energy  $\Delta E_X^{CORR}$  also decrease with increasing electric field and since they appear with a negative sign, changes in the single-particle energies are compensated. This behavior is the explanation for the small Stark shift observed in Fig. 2. In a similar manner, the energy of the biexciton can be approximated by,  $E_{XX} = 2\epsilon_{00}^e + 2\epsilon_{00}^h + V_{ee}^0 +$

$V_{hh}^0 - 4V_{eh}^0 - \Delta E_X^{CORR}$ . The energies of photons emitted in transitions  $A_1$  and  $B_1$  correspond to the differences between this energy and those of the two single excitons:  $E_{A1, B1} = (\epsilon_{00}^e + \epsilon_{00}^h - V_{eh}^0 - \Delta E_X^{CORR} \pm \frac{\Delta AES}{2}) + (V_{ee}^0 + V_{hh}^0 - 2V_{eh}^0) - (\Delta E_X^{CORR} - 2\Delta E_X^{CORR})$ . In this expression, the first term is identical to the PL peak positions of the single excitons, only with opposite contribution from the AES, and the second term accounts for the Coulomb interactions between the two electron-hole pairs building the biexciton. At zero electric field this second term is approximately zero, since the repulsion between carriers of the same type is balanced by electron-hole attraction, and it is the third term, comparing the correlation corrections to those of the exciton, which defines the splitting between the PL lines of the two complexes. This third term is usually negative, resulting in biexcitonic PL peaks that appear at lower energies than those of single excitons. With increasing electric field, the first term is almost unchanged because of the competing single particle and electron-hole Coulomb terms. However, as the electrons and holes are separated, the electron-hole attraction decreases, driving the biexciton PL peak positions towards higher energies. For a sufficiently large electric field the interaction terms exactly cancel the correlation corrections, resulting in a degeneracy of the biexciton and exciton emission and allowing indistinguishable biexciton decay channels to be identified.

The authors would like to acknowledge the financial support of the Canadian Institute for Advanced Research, the Canadian Institute for Photonic Innovations, QuantumWorks and the Natural Sciences and Engineering Research Council.

- 
- [1] A. Shields, *Nature Photonics* **1**, 215 (2007).
  - [2] C. Santori *et al.*, *Nature* **419**, 594 (2002).
  - [3] N. Gisin *et al.*, *Rev. Mod. Phys.* **74**, 145 (2002).
  - [4] O. Benson *et al.*, *Phys. Rev. Lett.* **84**, 2513 (2000).
  - [5] A. K. Ekert, *Phys. Rev. Lett.* **67**, 661 (1991).
  - [6] C. H. Bennett *et al.*, *Phys. Rev. Lett.* **70**, 1895 (1993).
  - [7] N. Gisin and R. Thew, *Nature Photonics* **1**, 165 (2007).
  - [8] R. M. Stevenson *et al.*, *Nature* **439**, 179 (2006).
  - [9] N. Akopian *et al.*, *Phys. Rev. Lett.* **96**, 130501 (2006).
  - [10] M. Bayer *et al.*, *Phys. Rev. B* **65**, 195315 (2002).
  - [11] K. Kowalik *et al.*, *Appl. Phys. Lett.* **86**, 041907 (2005).
  - [12] B. D. Gerardot *et al.*, *Appl. Phys. Lett.* **90**, 041101 (2007).
  - [13] A. Grelich *et al.*, *Phys. Rev. B* **73**, 045323 (2006).
  - [14] P. Hawrylak, *Solid State Commun.* **127**, 793 (2003).
  - [15] P. Hawrylak, *Phys. Rev. B* **60**, 5597 (1999).
  - [16] M. Bayer *et al.*, *Nature* **405**, 923 (2000).
  - [17] J. Lefebvre *et al.*, *J. Vac. Sci. Technol. B* **20**(5), 2173 (2002).
  - [18] V. Stavarache *et al.*, *Appl. Phys. Lett.* **89**, 123105 (2006).
  - [19] M. Korkusiński, M. E. Reimer, P. Hawrylak, and R. L. Williams. Unpublished.